NASA Technical Memorandum 102486

Comparison of Currents Predicted by NASCAP/LEO Model Simulations With Elementary Langmuir-Type Bare Probe Models for an Insulated Cable Containing a Single Pinhole

Joel T. Galofaro
Lewis Research Center
Cleveland, Ohio

July 1990

NASA

COMPARISON OF CURRENTS PREDICTED BY NASCAP/LEO MODEL SIMULATIONS WITH ELEMENTARY LANGMUIR-TYPE BARE PROBE MODELS FOR AN INSULATED CABLE CONTAINING A SINGLE PINHOLE

Joel T. Galofaro
National Aeronautics and Space Administration
Lewis Research Center
Cleveland, Ohio 44135

SUMMARY

The behavior of a defect in the insulation of a short biased section of cable in a low Earth orbit (LEO) space environment was examined. Such studies are of the utmost importance for large space power systems where great quantities of cabling will be deployed. An insulated probe containing a pinhole was placed into a hypothetical high-density LEO plasma. The NASA charging analyzer program (NASCAP/LEO) was used to explore sheath growth about the probe as a function of applied voltage and to predict I-V behavior. A set of independent current calculations using Langmuir's formulations for concentric spheres and coaxial cylinders were also performed. The case of concentric spheres was here extended to include the case of concentric hemispheres. Several simple Langmuir-type models were then constructed to bracket the current collected by the cable. The space-charge sheath radius and impact parameters were used to determine the proper current regime. I-V curves were plotted for the models and comparisons were made with the NASCAP/LEO results. Finally, the NASCAP/LEO potential contours and surface cell potential plots were examined to explain interesting features in the NASCAP/LEO I-V curve.

INTRODUCTION

The collection of current by a partially insulated probe has been a long-standing area of study in many spacecraft/plasma interaction processes. All spacecraft incorporate a large number of dielectric surfaces for thermal control (e.g., shuttle heat tiles) and for electrical power generation (e.g., solar cell arrays). Large dielectric surfaces can be differentially charged along their length because of locally variable incident-charged particle fluxes. Staskus (ref. 1), for example, has observed arc discharging between the 15-cm- and 20-cm-square tiles from the space shuttle thermal protection system exposed to monoenergetic multi-KeV electron beams.

Exposed conducting surfaces present quite a different problem in spacecraft charging, especially at the interfaces between adjacent insulator/conductor surfaces. Here, for example, Snyder (ref. 2) observed arcing between fused silica cover slides and silver interconnects that were biased between -500 to -1400 V.

Conductors can either be biased or floated with respect to the spacecraft floating potential. Floating conductors are uninteresting because they tend to charge only to a negative potential of a few kT with respect to the plasma

potential. This is due to the difference in the mobility of each charge species present; electrons possess a much greater mobility than do ions by virtue of their lower atomic mass. By contrast, conductors biased with respect to spacecraft ground act as current sinks, creating field-intensive regions which promote the collection of large currents.

All space plasmas have a tendency to remain electrically neutral. A slight imbalance in the space-charge density gives rise to strong electrostatic forces which act to restore electrical neutrality in the plasma. In regions where the space plasma is subjected to strong electric fields, the plasma will attempt to readjust its charge distribution in order to shield itself from the field by forming a charge sheath. It should be evident that all spacecraft are intimately coupled to their plasma environment.

SYMBOLS

a	probe radius, m
a_{hem}	radius of hemisphere, m
a_{sph}	radius of sphere, m
E	energy, kT, eV
e	electronic or ionic charge, C
I	current, A
j_r	random thermal current density, A/m^2
k	Boltzmann constant, J/K
ℓ	probe length, m
m	mass of electron or ion, kg
N	plasma or number density, m^{-3}
P	impact parameter, m
q	electronic or ionic charge, C
R_o	effective sheath radius or thickness, m
r_o	space charge sheath radius or thickness, m
SA_{pin}	surface area of pinhole, m^2
SA_{subd}	surface area of pinhole in subdivided region, m^2
T	electron temperature, eV
V	potential, V

xmesh grid spacing, m

α dimensionless quantity derived by Langmuir

ε_o permittivity of free space, C/Pa

BACKGROUND

A striking phenomenon that has been a subject of great interest is the high currents collected through a pinhole in the dielectric covering a charged metal. Cole et al. (ref. 3) evidently were the first to report such an instance. This appears to have triggered a number of other papers looking into the same phenomenon (refs. 4 to 7).

Floating potential is measured with respect to a fixed potential in space called the plasma potential. The net current to a probe at its floating potential is zero (ref. 8). Therefore, a necessary condition for currents to be collected through a pinhole in a dielectric material is that the bias voltage of the substrate must not be equal to the floating potential. Hereafter, the substrate bias exposed by the pinhole will be referred to as the pinhole bias. If the bias voltage is allowed to go slightly negative of the floating potential, electrons will start to be repelled, and the net current collected through the pinhole will be due to ions. If the pinhole bias is made negative enough, the number of collected ions will become saturated, and only the ion current density Ji will be collected, resulting in a positive charge sheath. Alternatively, if the pinhole bias is allowed to go slightly positive to that of the floating potential, ions will start being repelled and more electrons than ions will be collected by the pinhole. If the pinhole bias is increased just past that of the plasma potential, the ions will redistribute themselves away from the immediate vicinity of the pinhole. A negative charge sheath will form, and the electron current density Je will be collected by the pinhole. Finally, if the pinhole bias is made even more positive, the pinhole will exhibit a rather complicated current-voltage relationship, depending upon the constituency and the bulk properties of the plasma.

Sudden sheath growth about a pinhole that is biased significantly above or below the plasma potential is often attributed to the onset of secondary electron emission (refs. 6 and 9). Because charged particles entering the sheath region are subject to motion constraints imposed on them by their own angular momentum electric field, a certain percentage of them will miss the pinhole completely and strike the dielectric at a nearby point. If the energy of the particle upon collision is above a certain energy threshold (determined by the bulk properties of the dielectric) and below a certain energy maximum, there is a high probability that more than one secondary electron will be liberated from the surface of the dielectric, causing the dielectric to charge positive. As the pinhole bias is increased, so too is the effective collecting area of this sheath, causing a yet greater number of high energy charged particles to enter the pinhole sheath region. As a result, more and more secondary electrons will be liberated, causing a positive surface charge sheath to form on the dielectric. This phenomenon will henceforth be called "snapover."

With the new era of space exploration before us, the advent of Space Station Freedom, and TSS-1 Electrodynamic Tether applications, large amounts of

insulated electrical cabling will be deployed in the construction and operation of these missions. Of increasing importance is the question of how such cables will perform in space, and, specifically here, how defects in the insulation might influence the behavior of a long insulated wire. This report looks into these issues by making use of the NASA charging analyzer program for low Earth orbit (NASCAP/LEO) developed for NASA. An insulated probe of appropriate geometry, containing a single pinhole, is defined and hypothetically placed into a known space environment. The code is then used to explore sheath growth around the probe as a function of potential. Next, a bare cylindrical probe model is presented and the I-V curves obtained by it are plotted for comparison against those obtained by the NASCAP/LEO. Finally, a means of calculating the current collected by a spherical and a hemispherical probe, each having the same effective area as that of the pinhole, is presented. These results are then compared with the current collected by the pinhole, as obtained from the NASCAP/LEO.

PROCEDURE

The NASCAP/LEO is a finite-element computer code designed expressly for the study of the electrostatic interaction between a spacecraft having charged surfaces and a cold dense plasma. Environmental parameters under the NASCAP/LEO are user-specified parameters that need to be input prior to the calculation. Surface cell currents and potentials are particularly sensitive to the environment, and some thought must therefore be given to accurately describing the plasma environment for the model in question. The plasma environmental parameters used here and for all subsequent runs were based on typical high-density (worst case) LEO plasmas. (Plasma density was set at $10^{12} m^{-3}$, electron temperature at 0.1 eV, ion mass was set to 2.656×10^{-26} kg for oxygen ions, and the sheath boundary potential was set at 0.0873 eV.) The NASCAP/LEO allows the user to specify the object geometry, material composition of conductors and insulators, conductor biases, scale size, and placement of the object to be modeled in the NASCAP/LEO primary grid space.

The object modeled consisted of a short section of a copper conductor covered by a thin Kapton insulating jacket. A single puncture through the insulating jacket exposed a small area of the underlying conductor. (Note: The surface area of the pinhole was much smaller than the surface area of the object.) The conductor was then biased in the code positively with respect to the plasma potential, while all the Kapton insulating surfaces were allowed to float. Initially, the insulating surfaces (for low conductor biases) were predicted to sit at a small negative potential relative to the plasma, and then to become more and more positive as the conductor bias increased. It was possible to keep track of how the charge sheath should propagate over the insulator surfaces by looking at all insulator surface potentials over a range of conductor biases between 1 and 1000 V.

Typical outputs from the NASCAP/LEO consisted of two-dimensional potential contour plots (Y-Z and X-Y views) in the space around the object at a given conductor bias, as defined in the primary grid computational space. Other types of numerical outputs for individual surface cells were also obtained. These consisted of surface cell number and surface cell potential and current at each given conductor bias. By adding up the individual currents going to each surface cell, the incident total current collected by the object could be

obtained. The total incident current to the object was then plotted against the conductor bias to obtain the object's I-V curve characteristics.

In order to verify the NASCAP/LEO results, several comparisons were made. The first of these comparisons involved the application of Langmuir's space-charge-limited current (SCLC) equation for parallel plates (ref. 10; table I, eqs. (1.a) and (1.b)) and his SCLC equation for bare coaxial cylinders (ref. 11; table I, eq. (3.a2)). Assuming both planar (ref. 12) and cylindrical-charge sheaths, these equations were solved for the space-charge sheath radius (SCSR): (1) the thickness between the bare cylindrical probe and a planar-charge sheath boundary (table I, eq. (1.c)) and (2) the space-charge sheath thickness between the bare cylindrical probe and the coaxial cylindrical-charge sheath boundary (table I, eq. (3.c)). Such SCSR determinations were a necessary step in finding the proper type of current collection regime that applies.

The relevancy of performing the above calculations should be clarified. What was being attempted was a direct and independent current calculation of the object previously defined under the NASCAP/LEO. These calculations were to be performed from first principals starting with Langmuir's formulations for the space-charge-limited current to a bare parallel plate, sphere, and cylinder. In order to understand how an insulated object with a pinhole collects current, we must understand how this current compares with a similar object of the same geometry and dimensions, but containing no insulating surfaces. Hence, we need to deal with bare probe equations. Because the NASCAP/LEO object being defined was an idealized object (constructed from a finite number of cubes of the same size) due to code limitations, it lacked the true geometry we were trying to model. Consequently, rather than finding the current to a bare object of length L of square cross section, we chose to approximate it by calculating the current to a bare cylinder of length L, having a surface area approximately equal to the NASCAP/LEO defined object.

Whenever planar conditions were assumed, that is, when the charge sheath was assumed to be locally parallel to each point on the surface, then the problem reduced to finding the SCSR, R_o (i.e., that distance between a biased planar anode on the surface of the object and a parallel charge sheath boundary). Fortunately, this problem was amenable to the type of solution Langmuir used for finding the maximum current between two biased parallel plates (ref. 12). As a result, table I, equation (1.c) may be used to estimate the SCSR for a probe of any geometry.

The next set of comparisons involved calculating the SCLC collected by an insulated cylindrical probe containing a single pinhole. Because the pinhole contained the only exposed conductor on the surface of the object, it was the region where the largest currents were collected, and so was the logical choice of places to model. For simplicity, the model only considered conducting surfaces, leaving all insulator surfaces untreated. The assumption was that the insulated portions of the probe would be at some small negative potential both far from and near to the pinhole if snapover effects were not considered. As a result, only the exposed conducting area caused by the pinhole was considered in the formulation of this model.

For the case of a pinhole whose surface area is very small compared with the rest of the object, one would suppose current collection to be defined by

a spherical or hemispherical geometry. As the scale size of the pinhole increases and the surface area of the pinhole becomes a more significant portion of the entire surface area, one would suppose current collection to be dependent upon the geometry of the exposed region.

This report attempts to calculate the space-charge-limited current flowing to an insulated conductor with a pinhole by employing both a bare conducting sphere and hemisphere, each having a surface area equal to the area of the pinhole. A close examination of the NASCAP/LEO object (fig. 1(b)) reveals the appropriate scale dimensions in the pinhole region. Figures 2 and 3 show the calculations used to find the radius of a sphere and hemisphere of equal surface area to the pinhole. In the hemispherical case where we used a slightly larger probe radius, we used Langmuir's spherical form of the equation for the current (table I, eq. (4.a2)), and cut the collected current in half (eq. (4.a1)). This was equivalent to doubling the surface area of the hemisphere so that we were effectively collecting current from a larger spherical geometry probe from which we only accepted half of the current. The comparisons here involved the application of Langmuir's SCLC equations for parallel plates (table I, eqs. (1.a) and (1.b)), Langmuir's SCLC equation for concentric spheres (table I, eq. (2.a2)), and the subsequently derived expression for the SCLC equation for concentric hemispheres (table I, eq. (4.a2)). Assuming both planar- and spherical-type charge sheaths for the bare spherical pinhole model, Langmuir's bare concentric sphere SCLC expression for the SCSR was solved for the thickness between: (1) a bare sphere and a locally parallel planar charge sheath boundary (table I, eq. (1.c)) and (2) a bare sphere and a concentric spherical charge sheath boundary (table I, eq. (2.c)). The last comparison assumed a hemispherical-type charge sheath for the bare hemispherical pinhole model. A solution was found for equation (4.a2) in table I for the SCSR, the thickness between a bare hemispherical collector and a concentric hemispherical sheath boundary (table I, eq. (4.c)). After finding the SCSR for each case above, the applicable current collection regime was determined. Then I-V curves were plotted for each of the above pinhole models.

Table I lists all the relevant equations cited previously. Although many of the equations compiled under this table can be readily obtained from a number of sources, to the best of this author's knowledge this appears to be the first time all pertinent equations have been presented in a single location. Because Langmuir's original works (refs. 10 and 11) only extend over the cases of the parallel plates, coaxial cylinders, and concentric spheres, the concentric hemispherical equations presented in the table are newly derived. Fortunately, this was easily accomplished because the sphere and the hemisphere share the same geometry, and only minor changes had to be incorporated into the case of Langmuir's concentric spheres to make them applicable to the hemispherical case. It should be noted that a minor error was found in Langmuir's expression for the current between concentric spheres (ref. 10). His quoted parameters for D (for ions and electrons) could not be found as stated because of an inconsistency in the dimensions of his current equation. The error appears to have been propagated from the differences between the Gaussian and rationalized MKS units. Inclusion of a term for the permittivity of free space in the product of his current term rectifies the situation. All units for the equations in table I have been given in rationalized MKS so as to avoid any confusion as to which system is being used.

As stated previously, before any I-V curves could be calculated for the current collected by any of the geometries listed above, we first needed to

know which type of current collection regime applied at a given potential bias. We have already presented the calculations for one type of current collection regime, namely, the space-charge-limited current regime. The only other type of current collection that could apply was the so-called orbit-limited current regime.

Whereas the space-charge-limited current is determined by the modification of the electric field near the sheath boundary (as a result of the space charge of electrons in that region), the orbit-limited current collection is dominated by the orbital motion of electrons captured by the sheath. For the orbit-limited case, the sheath radius is determined by the applied potential, the electron temperature, the angle of incidence upon entering the sheath, and additionally, the radius of the probe. Therefore, electrons entering the sheath will either have (1) too little energy to escape the sheath region and will end up striking the probe, (2) too great an energy to be captured, but will still strike the probe because of their trajectory, or (3) too great an energy to be captured and will miss the probe completely, leaving the sheath region altogether. The impact parameter is used to determine the sheath thickness for the orbit-limited case.

The equation in table II defines the impact parameter and gives us a means of calculating the type of current collection regime that applies at a given potential bias. First, the type of geometry is chosen. Next, the space-charge sheath radius for that geometry and the impact parameter are calculated and the two values are compared. When the space-charge sheath radius is less than the impact parameter, a space-charge-limited calculation holds. Equations (5.1a) through (5.4a) in table II are then used to calculate the current. When the impact parameter is less than the space-charge sheath radius, an orbit-limited calculation holds, and equations (5.1b) through (5.4b) may be used to estimate the collected current. Finally, when the space-charge sheath radius is equal to the impact parameter, either set of formulations may be used for the current. This procedure was carried out for the range of potentials to be used in the NASCAP/LEO simulation. I-V curves were then obtained for direct comparisons with the NASCAP/LEO curve.

RESULTS

Figures 4(a) to (e) show a comparison of the space-charge sheath radius R_o and the impact parameter P versus the applied voltage V for five different sheath thickness approximations. The first of these approximations (fig. 4(a)) plots R_o,P versus V by using a planar sheath approximation (table I, eq. (1.c)) for R_o. The second type of approximation (fig. 4(b)) uses a cylindrical sheath approximation (table I, eq. (3.c)) for R_o. Figures 4(c) to (e) also plot R_o,P versus V but use planar (table I, eq. (1.c)), spherical (table I, eq. (2.c)), and hemispherical (table I, eq. (4.c)) approximations, respectively, for the space-charge sheath radius R_o.

It should be noted that the plots of R_o,P in figures 4(a) to (e) are dependent upon the particular probe geometry and the probe radius a. The bare cylindrical probe models, which use a planar (fig. 4(a)) and a cylindrical charge sheath thickness approximation (fig. 4(b)) for R_o, have the same probe geometry and probe radius. Here the radius has been set equal to 1/2 the grid spacing (xmesh) used in the NASCAP/LEO object or $a = 1.5875 \times 10^{-3}$ m. The

spherical pinhole models using planar (fig. 4(c)) and spherical (fig. 4(d)) space-charge sheath thickness approximations for R_O also use the same value for the probe radius $a = 2.2391 \times 10^{-4}$ m, as determined in figure 2. The final hemispherical pinhole model uses a hemispherical charge sheath thickness approximation (fig. 4(e)) for R_O and uses the value of the probe radius $a = 3.1666 \times 10^{-4}$ m, which is derived in figure 3.

Inspection of figures 4(a) to (e) shows that R_O is greater than P at any specified voltage along each of the curves. Therefore, an orbit-limited calculation is correct for all Langmuir-type probe models considered.

Figure 5 shows a comparison of the currents collected by two different bare cylindrical probe models (curves e and f). Both of these models yield the same I-V curve. The same equation (table II, eq. (5.3b)) is used to compute the current collected by both bare cylindrical probe models here. Referring back to figures 4(a) and (b), one can see that the range of values for R_O varies considerably between the planar and cylindrical sheath thickness cases. One would, therefore, expect very different currents from each of these models were it not for the fact that neither of these sheath distances for R_O is used in the current calculations for these models because the orbit-limited regime applies in both cases. Because each of these models uses the impact parameter P (equation in table II) in its current calculations, this leads to the same value of P at a given voltage and to the same I-V curve in both of these models. It should also be noted that the plots of V versus P in figures 4(a) and (b) are actually the same curve by virtue of this equation. (Because of the rescaling of the Y-axis dimension to the maximum value of R_O in each case, P is plotted accordingly.) Similarly, figures 4(c) and (d) also yield the same value for P for the reasons indicated above.

In figure 5, curves a, b, and c show a comparison of the collected current between three different pinhole models. The resultant I-V curves are the same regardless of which of the probe models (spherical or hemispherical) is applied. What is also evident here is that the pinhole current collected by a bare spherical probe of equal surface area to that of the pinhole is about two orders of magnitude less than what would be collected by a noninsulated cylindrical probe of the same overall dimensions as the entire NASCAP/LEO object.

Consequently, the current collected by an insulated cylindrical probe containing a single pinhole has been bracketed. The actual current collected should fall somewhere between curves a, b, and c and curves e and f of figure 5. (Actually, one would suppose the collected current to be closer to curves a, b, and c, where the collecting surfaces are equal in area to that of the pinhole.)

Curve d in figure 5 shows the resultant I-V curves obtained from the NASCAP/LEO runs for an insulated cylindrical probe containing a single pinhole. This curve contains many noteworthy features. Up to about 600 V potential, the NASCAP/LEO curve appears to predict somewhat less current than either the spherical or hemispherical pinhole curves, although the current continues to converge to the 600 V NASCAP/LEO current throughout this range. (It should also be noted that in the potential range 25 to 115 V, the current collected by the spherical and hemispherical pinhole models is approximately a

factor of 4 greater than that predicted by the NASCAP/LEO model at any specified voltage within this range. The reason for this discrepancy will be explained in the conclusions.) In the range 130 to 600 V, the current from the spherical/hemispherical pinhole models and the NASCAP/LEO curves appear to slash converge with one another. In the voltage range 620 to 680 V, the spherical and hemispherical pinhole models collect nearly the same amount of current as predicted by the NASCAP/LEO simulation. In the potential range 685 to 1000 V, the NASCAP/LEO curve appears to collect about a factor of 4 greater current than the spherical or hemispherical pinhole curves.

There are also several knee regions on the NASCAP/LEO curve where the current collection changes rather sharply. These regions occur from 100 to 130 V, 600 to 640 V, and 680 to 700 V potential and can be attributed to the snapover phenomenon.

The analysis begins by looking at NASCAP/LEO-generated contour plots of equipotentials and plots of surface cell potentials in each of the specified voltage regions above. The position of the zero-potential contour line with respect to the pinhole, as well as changes in the insulator surface cell potentials, are used as an indicator of the extent of the sheath edge or boundary. Thus, drastic changes in the position of the sheath boundary should signal that snapover is occurring or has occurred.

Figures 6(a) to 14(a) show a face-on view of an x-z cutplane slicing through the pinhole. Figures 6(b) to 14(b) show a cross-sectional end-on view of an x-y cutplane slicing through the pinhole. Figures 6(c) to 14(c) show a close-in view of the subdivided region, with all surface cells labeled and surface potentials plotted. Figures 6(d) to 14(d) show a full object view of the cable with all corresponding surface cell potentials and cell numbers plotted.

Two contour plots (figs. 6(a) and (b)) show that the sheath, which propagates from the pinhole, looks like a narrow ring of charge at 75 V potential. The corresponding surface potential maps (figs. 6(c) and (d)) show nothing out of the ordinary. At 100 V potential, the contour plots (figs. 7(a) and (b)) show only a slight expansion in sheath size. However, the corresponding surface cell potential maps show (fig. 7(c)) for the first time that the potential on the pinhole's nearest neighboring surface cells has undergone a sign change. The voltage on these cells has changed from slightly under -1 V to something in the range of +1 V. This appears to be the first evidence that snapover has begun. Next, at 130 V potential, figures 8(a) and (b) show that the sheath edge has grown considerably. The x-y cross-sectional view (fig. 8(b)) shows that the sheath boundary has begun to wrap around the object past the front surfaces. Figure 8(c) demonstrates that snapover is indeed occurring. The surface cell potentials of adjacent, nearest neighboring cells have increased greatly. This coincides with the sharp change in current predicted by the NASCAP/LEO curve (fig. 5, curve d) between 100 and 130 V potential. By 600 V potential, it is evident that the sheath edge (zero-potential contour line) completely surrounds the object (fig. 9(b), x-y view) and that the 0.1 V potential contour line wraps around three sides of the object. The surface cell potentials (fig. 9(c)) at this point are nearly all positive, except for the concentric ring of cells about the center and each of the surface cells on the right and left sides of the pinhole which are still between -1 and 0 V potential. Evidently, secondary electron focusing due to the applied field seems to be the cause here. All other surface cells outside of the subdivided region (fig. 9(d)) still appear to be at a small negative potential. At 620 V

potential, the +0.1 V potential contour line has completely snapped around the object (fig. 10(b)). The zero-volt potential contour line (fig. 10(a)) appears to start growing along the length of the cylinder outward from the pinhole center. In figure 10(c), the surface cell potential map at 620 V potential clearly demonstrates that most surface cells within the subdivided region have dramatically increased in potential. This coincides with the sharp jump in current collection between 600 and 620 V on the NASCAP/LEO predicted I-V curve. All surface cells outside of the subdivided region, however, still remain at a small negative potential. At 680 V potential there appears to be no significant change in either the contour plots or surface cell potential maps (figs. 11(a) to (d)). Finally, figures 12(a) and (b) show significant changes in sheath structure. It seems that the pinhole at this point begins to collect current like a larger bare sphere, as borne out by figures 12(a) and (b) and the NASCAP/LEO I-V curve at this voltage. It is also evident from figures 12(c) and (d) that considerable changes have taken place here also. For the first time we see that the surfaces of two cells on the top and bottom faces of the cable (outside the subdivided region) are beginning to grow to a substantial positive potential. This appears to account for the observed current shift between 680 and 685 V potential.

Although there are no sharp changes in the current collected by the NASCAP/LEO I-V curve for the voltage range 690 to 1000 V, for the sake of completeness, plots are presented in the 800 and 1000 V potential region. At 800 V potential, figure 13(d) shows that the cell potentials of two adjacent cells (one cell flanking each side of the subdivided region on the front face of the cable) have charged to a slightly positive potential. This indicates that a positive charge sheath is beginning to grow over these surfaces along the length of the cable. The 1000-V surface cell potential map (fig. 14(d)) shows the same features with the only difference being that the voltage of the two adjacent cells has greatly increased.

CONCLUSIONS

The NASCAP/LEO I-V curve (fig. 5) demonstrates that there are a number of different types of snapover effects occurring throughout the applied voltage range (as opposed to just one type occurring throughout the entire pinhole bias voltage region as previously thought). Indeed, three such snapover effects were found in the present cable simulation and there could conceivably be more at higher bias voltages. At 1000 V potential, the majority of surface cells outside the subdivided region remain at approximately -1 V potential. It is therefore conceivable that, at some higher potential when all insulated surface cells become charged positive, there could be yet another large shift in current collection. It is also conceivable that probe geometry, sharp edges, and pinhole size could have an effect on the exact number of snapover effects observed.

The first type of snapover effect occurs between 100 and 130 V where the charge sheath first jumps to the insulator surfaces in the adjacent vicinity of the pinhole. This is probably due to the onset of significant secondary electron emissions in this voltage region.

The second type of snapover effect occurs between 600 and 620 V, where the positive-charge sheath in space completely surrounds the radius of the cable (as evidenced by the x-y view of the +0.1 contour line in fig. 10(b)).

The second type of snapover effect appears to be a necessary precursor to the third type of snapover effect observed.

The third and final type of snapover effect seems to be an edge effect occurring between 680 and 685 V potential. It is here that the positive-charge sheath has propagated from the front face to the sides of the cable and so is termed the "snap-around effect." In a perfect cylindrical cable with no sharp edges, this effect would probably not be seen until the positive-surface-charge sheath has completely wrapped around the cylinder. One must also conclude from the surface potential maps and the resultant NASCAP/LEO I-V curve that the positive-surface-charge sheath must snap around the cable before it can grow along its length.

Particularly disturbing is the lower voltage region (0 to 100 V potential) where the NASCAP/LEO predicts about a factor of 4 lower current than any of the Langmuir-type pinhole models (LTPM). Because the NASCAP/LEO and the LTPM's solve Poisson's equation, and because snapover effects are not applicable at lower voltages, it was assumed that the NASCAP/LEO predicted values would yield the same result as the LTPM's. The reason that they do not agree is that the NASCAP/LEO simulation assumes space-charge-limited currents where, in fact, the LTPM's have shown the current collection to be orbit-limited. For the case where the Debye length is greater than the pinhole dimensions, many of the particles traced through the sheath boundary will miss the pinhole completely. As a result, less current is predicted by the current NASCAP/LEO simulations than by the LTPM approximations.

Langmuir-type probe models that attempt to bracket the NASCAP/LEO current solutions (for an insulated cable with a pinhole) appear to suggest that current collection should favor an orbit-limited current calculation. Furthermore, for small object dimensions (on the order of a centimeter), it is evident that at lower voltages LTPM's more accurately predict collected current because the NASCAP/LEO only makes its calculations in the space-charge-limited current regime.

Overall (all low-voltage behavior aside), the Langmuir-type models (LTM's) do quite well in bracketing the current collected by an insulated cable with a pinhole. Here the bare spherical and hemispherical LTM approximations, while not able to predict the sharp changes in current observed in the NASCAP/LEO-generated I-V curve, are within a factor of 4 of those values. The reason for this is clear. No bare probe model, however sophisticated, can hope to include secondary electron emission from the dielectric. Consequently, it is impossible for a bare probe model to predict snapover effects. Even so, the bare LTM approximations of the aforementioned geometries offer a reasonably good estimate of the current for a biased insulated probe with a pinhole without having to resort to a number of lengthy NASCAP/LEO computer runs. For this reason they are quite useful. They are also useful in understanding the NASCAP/LEO results.

REFERENCES

1. Staskus, J.V.: Electron Beam Charging of Space Shuttle Thermal Protection System Tiles. Spacecraft Environmental Interactions Technology 1983, NASA CP-2359, 1983, pp. 91-102.

2. Snyder, D.B.: Discharges on a Negatively Biased Solar Cell Array in a Charged Particle Environment. Spacecraft Environmental Interactions Technology 1983, NASA CP-2359, 1983, pp. 379-388.

3. Cole, R.K.; Ogawa, H.S.; and Sellen, J.M., Jr.: Operation of Solar Cell Arrays in Dilute Streaming Plasmas. (TRW-09357-6006-R000, TRW Systems; NASA Contract NAS3-10612), NASA CR-72376, 1968.

4. Grier, N.T.; and McKinzie, D.J., Jr.: Current Drainage to a High Voltage Probe in a Dilute Plasma. NASA TM-X-67890, 1971.

5. Kennerud, K.L.: High Voltage Solar Array Experiments. NASA CR-121280, 1974.

6. Stevens, N.J.: Interactions Between Spacecraft and the Charged Particle Environment. Spacecraft Charging Technology 1978, NASA CP-2071, 1978, pp. 268-294.

7. Meulenberg, A.; and Robinson, P.A. Jr.: Conduction Through Punctures in Metal Backed Dielectrics. Spacecraft Charging Technology 1980, NASA CP-2182, 1980, pp. 342-352.

8. Reitz, J.R.; and Milford, F.J: Foundations of Electromagnetic Theory. 2nd ed., Addison-Wesley, Reading, ME, 1967, pp. 269-292.

9. Katz, I. et al.: A Three Dimensional Dynamic Study of Electrostatic Charging in Materials. (SSS-R-77-3367, Systems, Science and Software; NASA Contract NAS3-20119), NASA CR-135256, 1977.

10. Langmuir, I.; and Blodgett, K.B.: Current Limited by Space Charge Between Concentric Spheres. Phys. Rev., vol. 24, July 1924, pp. 49-59.

11. Langmuir, I.; and Blodgett, K.B.: Currents Limited by Space Charge Between Coaxial Cylinders. Phys. Rev., vol. 22, Oct. 1923, pp. 347-356.

12. Mandell, M.J.; Jongeward, G.A.; and Katz, I.: NASCAP/LEO Reference Manual. SSS-R-85-7300, NASA Contract Report, June 1985, pp. 4-9.

TABLE I. - SPACE-CHARGE-LIMITED EQUATIONS FOR A PARALLEL PLATE, CONCENTRIC SPHERES AND HEMISPHERES, AND COAXIAL CYLINDERS.

[All specified relations are in MKS units; $j_r = Ne\sqrt{kTe/2\pi m}$; $R_o = r_o + a$.]

Bare probe geometry	Current, I, A	Random thermal current density, j_r, A/m^2	Thick sheath approximation Space-charge sheath radius, r_o, m
II Flat plates	Chen: (1.a)† $I = j_r$	Child (1.b)†* $j_r = \frac{4\epsilon_o}{9}\sqrt{\frac{2e}{m}}\frac{V^{3/2}}{r_o^2}$	(1.c)* $r_o = \underbrace{\left[\left(\frac{8\epsilon_o}{9e}\right)^2 \pi\right]^{1/4}}_{9330} \frac{V^{3/4}}{\sqrt{N}(kT)^{1/4}}$
Concentric spheres	Chen: (2.a1)† $I = 4\pi r_o^2 j_r$ Langmuir: (2.a2) $I = \frac{4\sqrt{2\epsilon_o}}{9}\sqrt{\frac{e}{m}}\frac{V^{3/2}}{\alpha^2}$ Smaller sphere Kennerude: (2.a3) $\alpha^2 = 1.16\,(r_o/a)^{3/2}$	(2.b)†* $j_r = \frac{\epsilon_o}{9\pi}\sqrt{\frac{2e}{m}}\frac{V^{3/2}}{r_o^2\alpha^2}$	(2.c)* $r_o = \underbrace{\left[\frac{2\epsilon_o}{\sqrt{109\pi e}}\right]^{2/7}}_{86.31} \frac{(aV)^{3/7}}{N^{2/7}(kT)^{1/7}}$
Coaxial cylinders	Langmuir: (3.a1)† $I = 2\pi r_o \ell j_r$ (3.a2) $I = 8\pi\ell\epsilon_o\sqrt{\frac{e}{m}}\frac{V^{3/2}}{r_o(\ell n r_o/a)^2}$	(3.b)†* $j_r = \frac{4\epsilon_o}{9}\sqrt{\frac{2e}{m}}\frac{V^{3/2}}{r_o^2(\ell n r_o/a)^2}$	(3.c)* $r_o \ell n(r_o/a) = \underbrace{\left[\left(\frac{8\epsilon_o}{9e}\right)^2 \pi\right]^{1/4}}_{9330} \frac{V^{3/4}}{\sqrt{N}\,(kT)^{1/4}}$
Concentric hemispheres Note: a is the same value for spheres and hemispheres.	(4.a1)† $I = 2\pi r_o^2 j_r$ (4.a2) $I = \frac{4\sqrt{2\epsilon_o}}{9}\sqrt{\frac{e}{m}}\frac{V^{3/2}}{\alpha^2}$ Larger sphere (4.a3) $\alpha^2 = 1.16(r_o/\sqrt{2}a)^{3/2}$	(4.b)†* $j_r = \frac{2\epsilon_o}{9\pi}\sqrt{\frac{2e}{m}}\frac{(\sqrt{2}aV)^{3/2}}{r_o^2\alpha^2}$	(4.c)* $r_o = \underbrace{\left[\frac{4\epsilon_o}{\sqrt{109\pi e}}\right]^{2/7}}_{105.21} \frac{(\sqrt{2}aV)^{3/7}}{(N)^{2/7}(kT)^{1/7}}$

†These relations are for electrons of mass m. For ions multiply R.H.S. of current by $\sqrt{m/M}$, M being the mass of the ions.
*All values of kT are in units of eV.

TABLE II. - DETERMINATION OF SPACE-CHARGE-LIMITED OR ORBIT-LIMITED CURRENTS FOR PLANES, SPHERES, CYLINDERS, AND HEMISPHERES

[Impact parameter, P, cm = a $\sqrt{1 + qV/\varepsilon}$.]

Space-charge-limited current	$P > R_o > P$	Orbit-limited current
(5.1a) $I = j_r$	Planar geometry	(5.1b) ----------
(5.2a) $i = 4\pi R_o^2 j_r$	Spherical geometry	(5.2b) $i = 4\pi P^2 j_r$
(5.3a) $i = 2\pi R_o \ell j_r$	Cylindrical geometry	(5.4b) $i = 2\pi P \ell j_r$
(5.4a) $I = 2\pi R_o^2 j_r$	Hemispherical geometry	(5.4b) $I = 2\pi P^2 j_r$

XMESH = 1/8 IN. = .093175 M

DIMENSIONS:	X	Y	Z		
	1	1	30	KAPTON	120 SURFACE CELLS (-2 CELLS IN SUBDIVIDED REGION)
SUBDIVIDED REGION: (2 SURFACE CELLS)	0	8	16	KAPTON	124 SURFACE CELLS
(PINHOLE)		2	2	GOLD	4 SURFACE CELLS

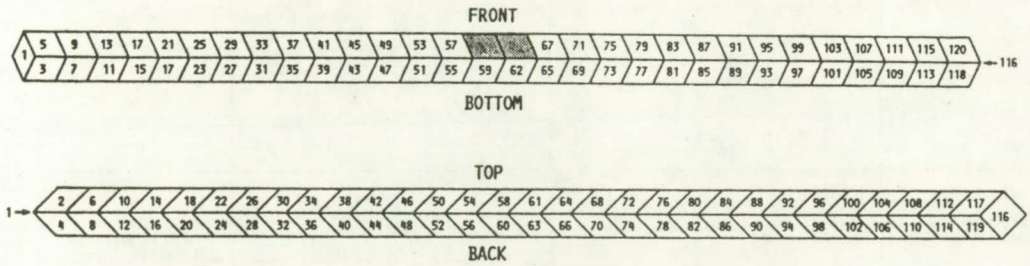

(a) FULL VIEW.

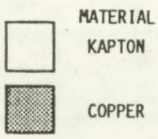

229	230	231	232	233	234	235	236	237	238	239	240	241	242	243	244
213	214	215	216	217	218	219	220	221	222	223	224	225	226	227	228
197	198	199	200	201	202	203	204	205	206	207	208	209	210	211	212
183	184	185	186	187	188	189	247	248	190	191	192	193	194	195	196
169	170	171	172	173	174	175	245	246	176	177	178	179	180	181	182
153	154	155	156	157	158	159	160	161	162	163	164	165	166	167	168
137	138	139	140	141	142	143	144	145	146	147	148	149	150	151	152
121	122	123	124	125	126	127	128	129	130	131	132	133	134	135	136

(b) EXPANDED VIEW OF SUBDIVIDED REGION WITH PINHOLE.

Figure 1.—NASCAP/LEO cylindrical object with pinhole.

XMESH = 1/8 IN. = 3.175×10^{-3} M

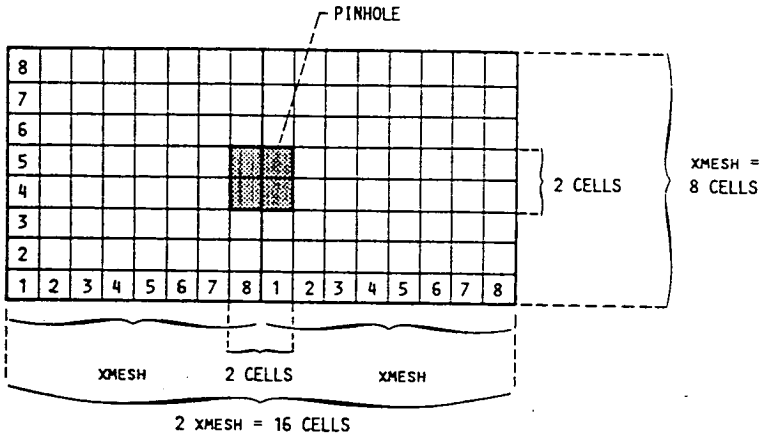

TOTAL NUMBER OF CELLS IN SUBDIVIDED REGION = 8 x 16 = 128 CELLS

TOTAL NUMBER OF CELLS IN PINHOLE = 4 CELLS

TOTAL SURFACE AREA OF SUBDIVIDED REGION = SA_{SUBD} = (2) (XMESH) (XMESH)

SURFACE AREA OF PINHOLE = $SA_{PIN} = \frac{4}{128}$ (2) $(XMESH)^2$

SURFACE AREA OF SPHERE = $4\pi a^2 = SA_{PIN}$ $\qquad a_{SPH}$ = SPHERE RADIUS

$SA_{SPH} = SA_{PIN}$

FINDING RADIUS (a) OF A SPHERE OF EQUAL SURFACE AREA TO THAT OF THE PINHOLE IN NASCAP/LEO OBJECT

$SA_{PIN} = 4\pi a^2$

$$a_{SPH} = \sqrt{\frac{SA_{PIN}}{4\pi}} = \frac{XMESH}{8\sqrt{\pi}} = 2.23912 \times 10^{-4} \text{ M}$$

Figure 2.—Calculations for radius of sphere of equal surface area to pinhole in NASCAP/LEO defined object.

FINDING THE RADIUS OF A HEMISPHERE (a_{HEM}) OF EQUAL SURFACE AREA (SA) TO A SPHERE OF RADIUS (a_{SPH})

SURFACE AREA OF SPHERE = SA_{SPH}

SURFACE AREA OF HEMISPHERE = SA_{HEM}

LET:

$$SA_{SPH} = SA_{HEM} = SA_{PIN}$$

THEN:

$$\left.\begin{aligned} SA_{SPH} &= 4\pi a^2_{SPH} \\ SA_{HEM} &= 2\pi a^2_{HEM} \end{aligned}\right\} \quad \text{WHERE:} \quad SA_{PIN} = \frac{XMESH^2}{16}$$

THEREFORE:

$$a_{SPH} = \frac{XMESH}{8\sqrt{\pi}} \quad \text{AND} \quad a_{HEM} = \frac{XMESH}{4\sqrt{2\pi}}$$

$$\frac{a_{HEM}}{a_{SPH}} = \sqrt{2} \quad \text{OR} \quad a_{HEM} = \sqrt{2}\ a_{SPH} = 3.16659 \times 10^{-4} \text{ M}$$

Figure 3.—Calculations for radius of hemisphere of equal surface area to pinhole in NASCAP/LEO defined object.

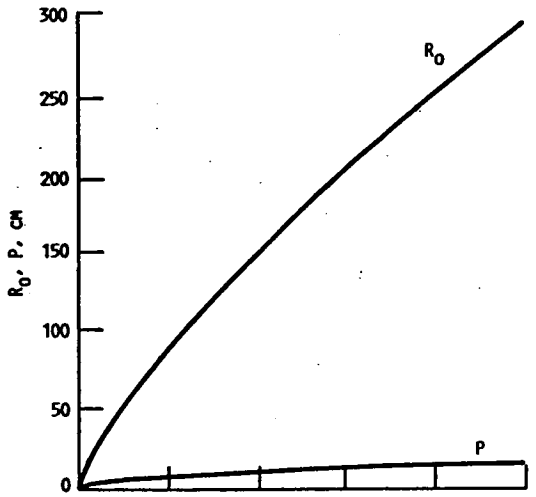

(a) FOR BARE CYLINDRICAL PROBE USING A PLANAR SHEATH GEOMETRY FOR R_0.

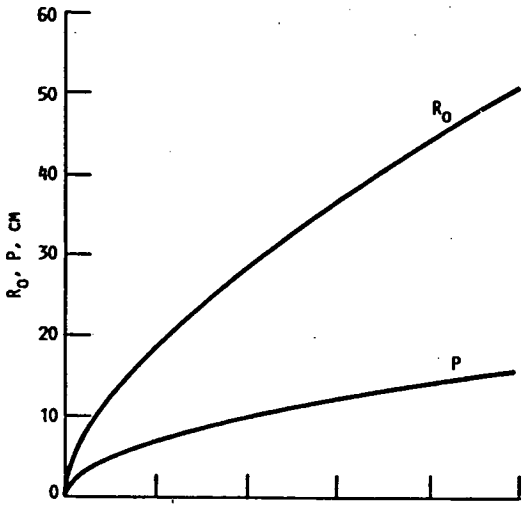

(b) FOR BARE CYLINDRICAL PROBE USING A CYLINDRICAL SHEATH GEOMETRY FOR R_0.

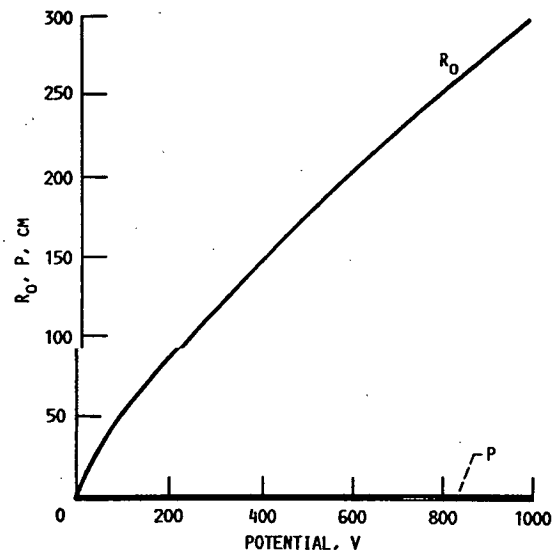

(c) FOR BARE SPHERICAL PINHOLE USING A PLANAR SHEATH GEOMETRY FOR R_0.

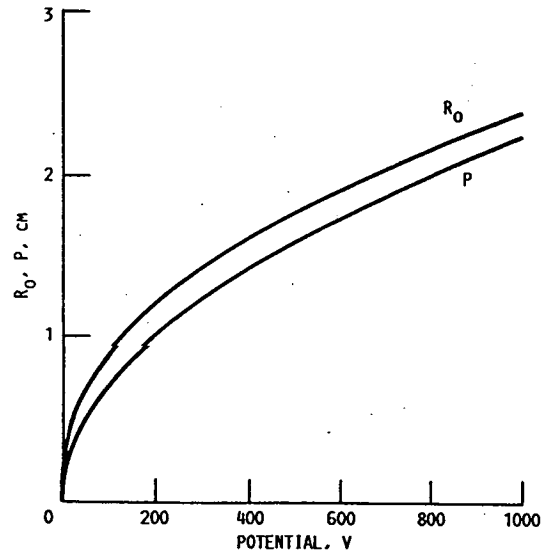

(d) FOR BARE SPHERICAL PINHOLE USING A SPHERICAL SHEATH GEOMETRY FOR R_0.

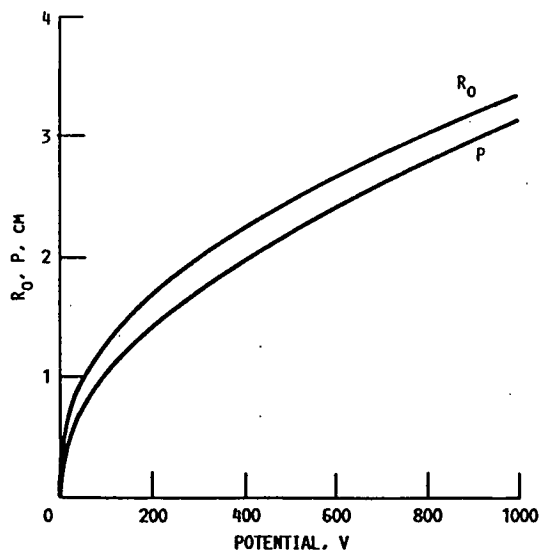

(e) FOR BARE HEMISPHERICAL PINHOLE USING A HEMISPHERICAL SHEATH GEOMETRY FOR R_0.

Figure 4.—Plots of applied voltage V vs space-charge sheath radius R_0 and impact parameter P.

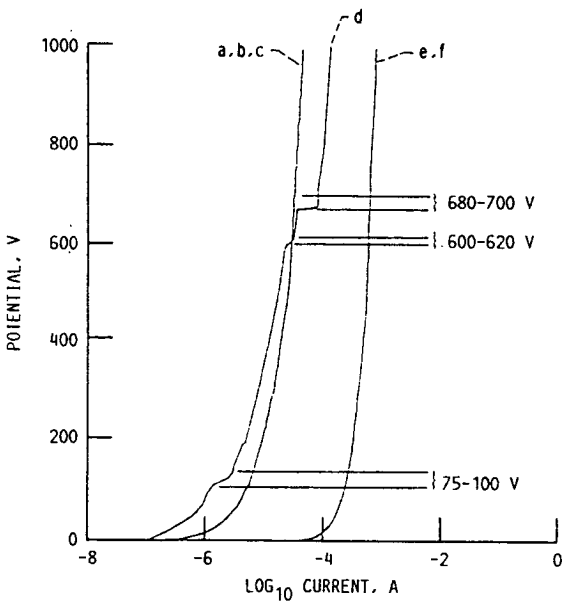

[a] ORBIT-LIMITED CURRENT RESULTING FROM A PLANAR SPACE-CHARGE SHEATH THICKNESS BEING APPLIED TO A SPHERICAL PINHOLE CURRENT.

[b] ORBIT-LIMITED CURRENT RESULTING FROM A SPHERICAL SPACE-CHARGE SHEATH THICKNESS BEING APPLIED TO A SPHERICAL PINHOLE CURRENT.

[c] ORBIT-LIMITED CURRENT RESULTING FROM A HEMISPHERICAL SPACE-CHARGE SHEATH THICKNESS BEING APPLIED TO A HEMISPHERICAL PINHOLE CURRENT.

[d] NASCAP/LEO PREDICTED CURRENT FOR AN INSULATED CABLE WITH A SINGLE PINHOLE.

[e] ORBIT-LIMITED CURRENT RESULTING FROM A PLANAR SPACE-CHARGE SHEATH THICKNESS BEING APPLIED TO A CYLINDRICAL PROBE CURRENT (SAME OVERALL DIMENSIONS AS NASCAP/LEO OBJECT).

[f] ORBIT-LIMITED CURRENT RESULTING FROM A CYLINDRICAL SPACE-CHARGE SHEATH THICKNESS BEING APPLIED TO A CYLINDRICAL PROBE CURRENT (SAME OVERALL DIMENSIONS AS NASCAP/LEO OBJECT).

Figure 5.—Comparison of collected currents between various Langmuir-type probe models and NASCAP/LEO values.

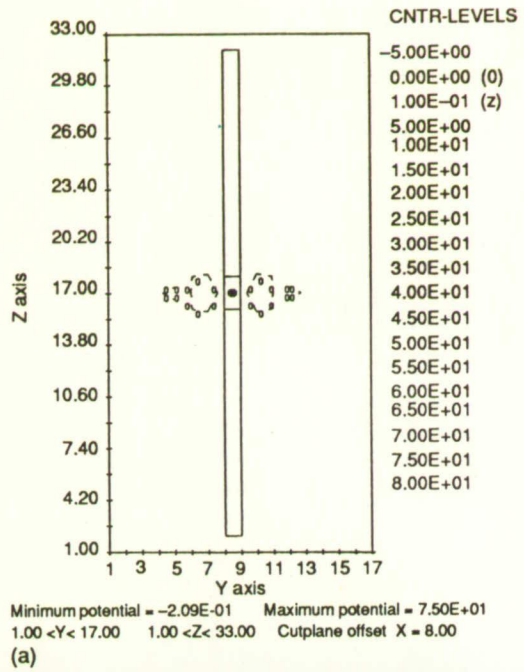

(a)

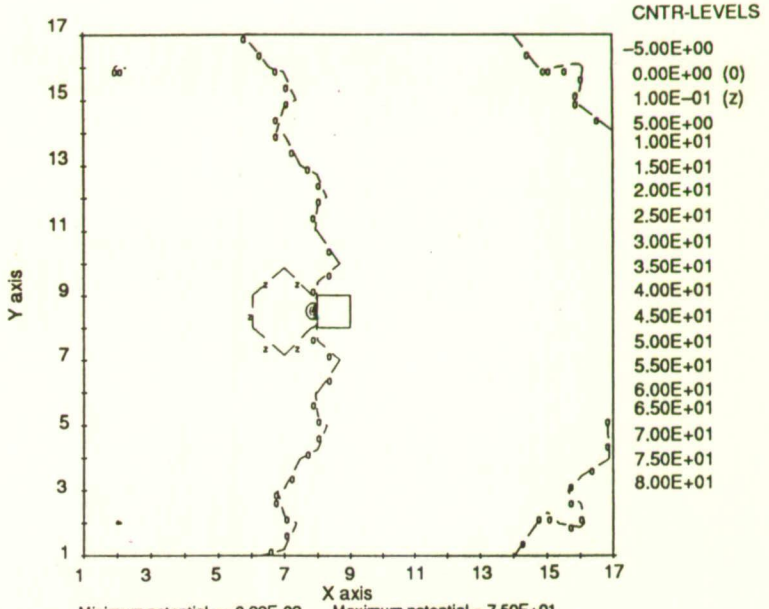

(b)

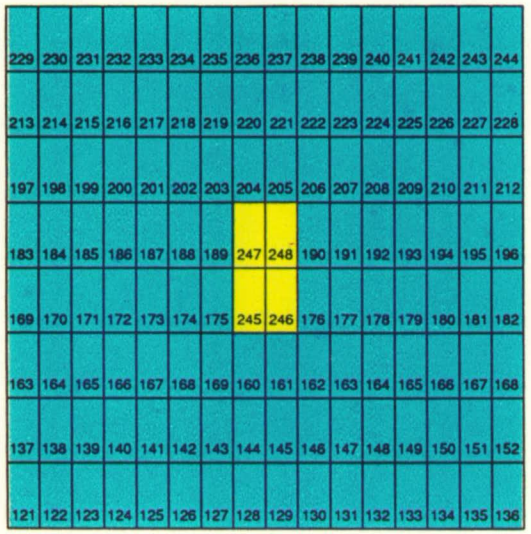

(c)

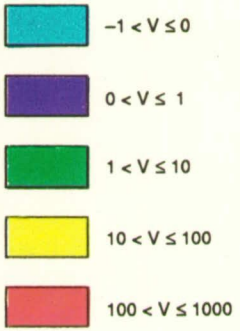

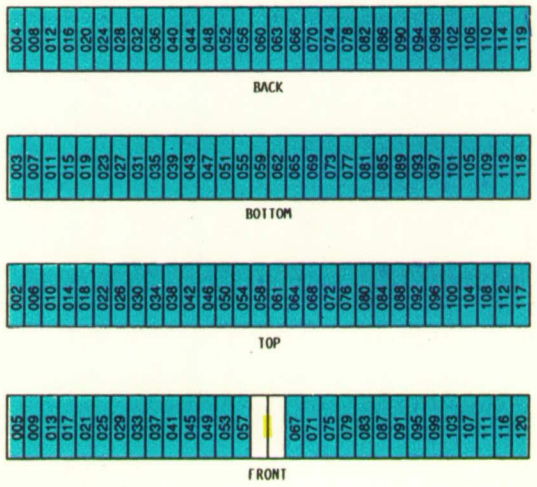

(d)

Figure 6.—Contour plots and surface cell potential maps for 75-V NASCAP/LEO run.

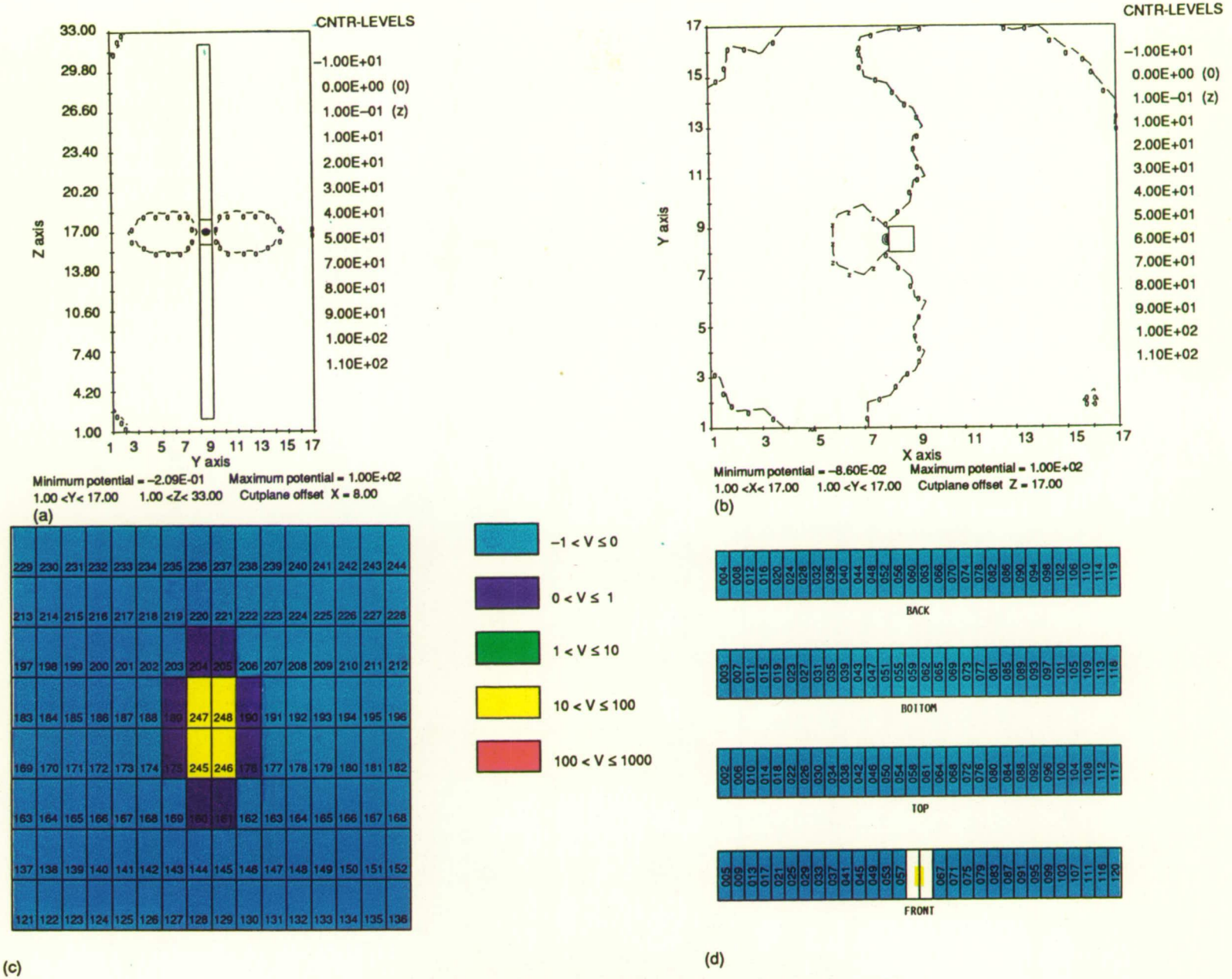

Figure 7.—Contour plots and surface cell potential maps for 100-V NASCAP/LEO run.

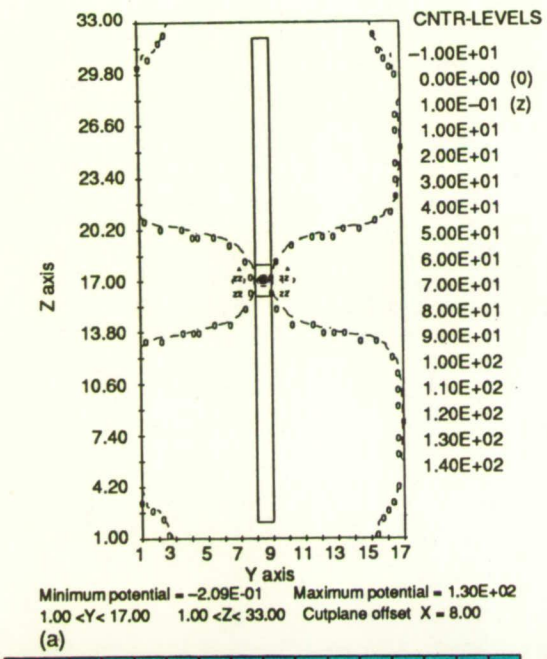

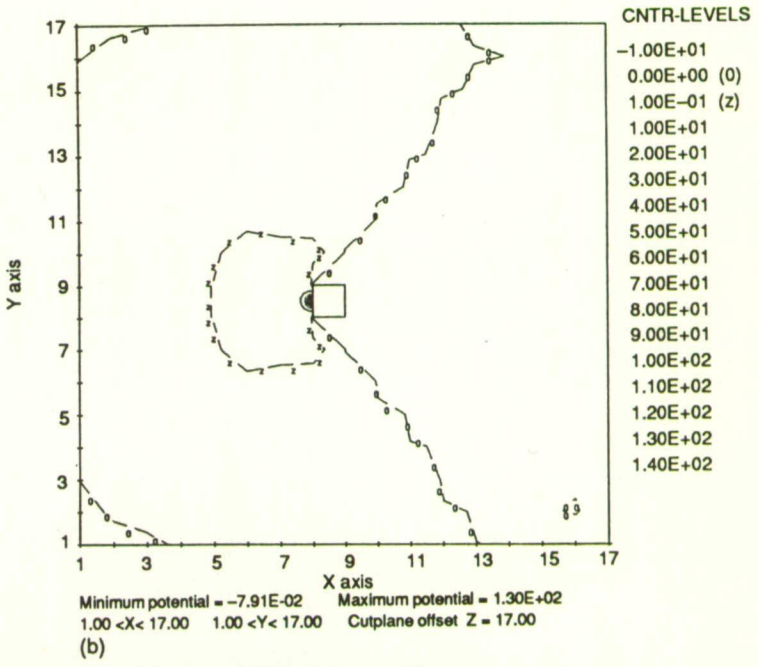

(c)

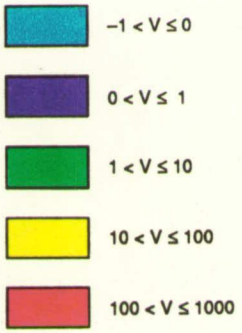

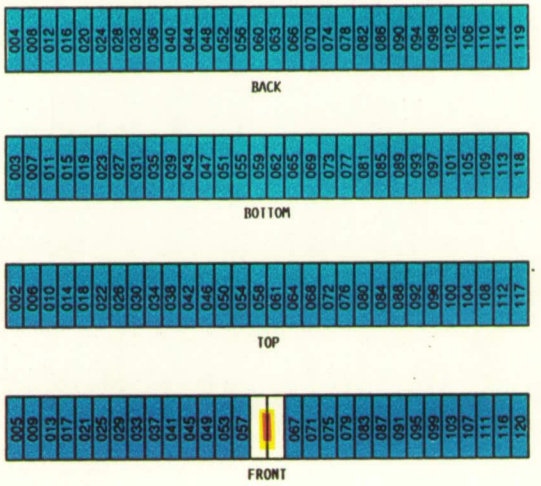

(d)

Figure 8.—Contour plots and surface cell potential maps for 130-V NASCAP/LEO run.

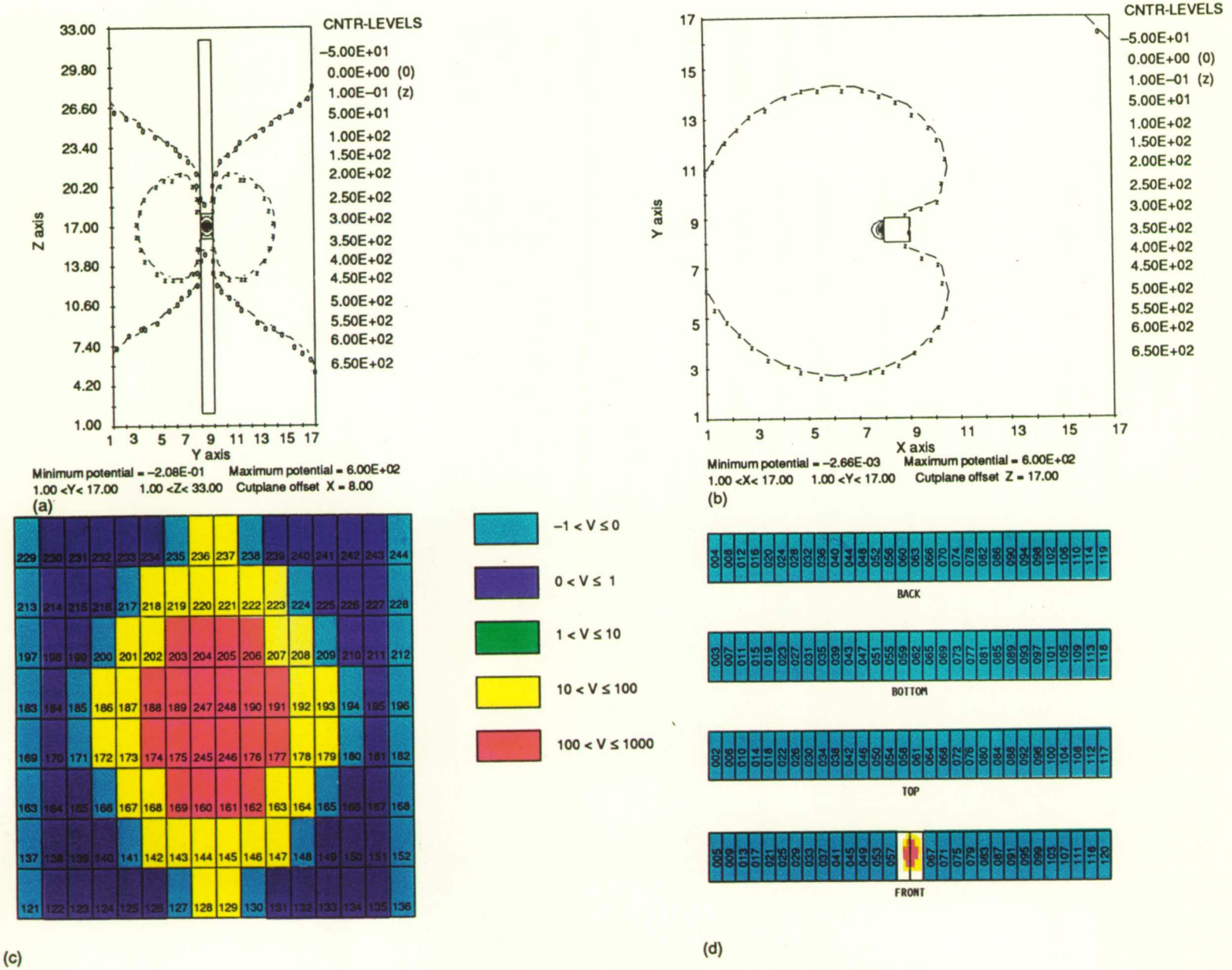

Figure 9.—Contour plots and surface cell potential maps for 600-V NASCAP/LEO run.

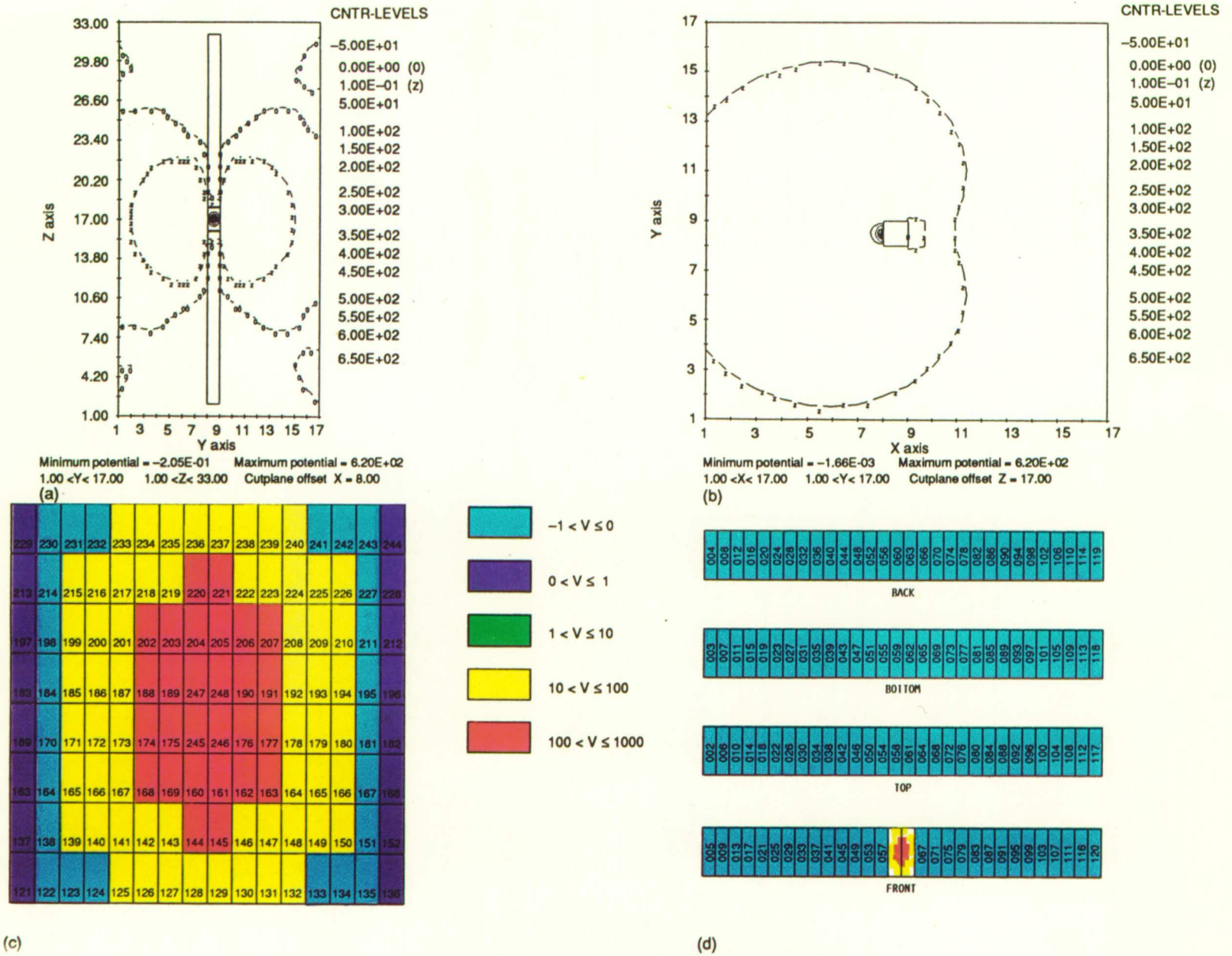

Figure 10.—Contour plots and surface cell potential maps for 620-V NASCAP/LEO run.

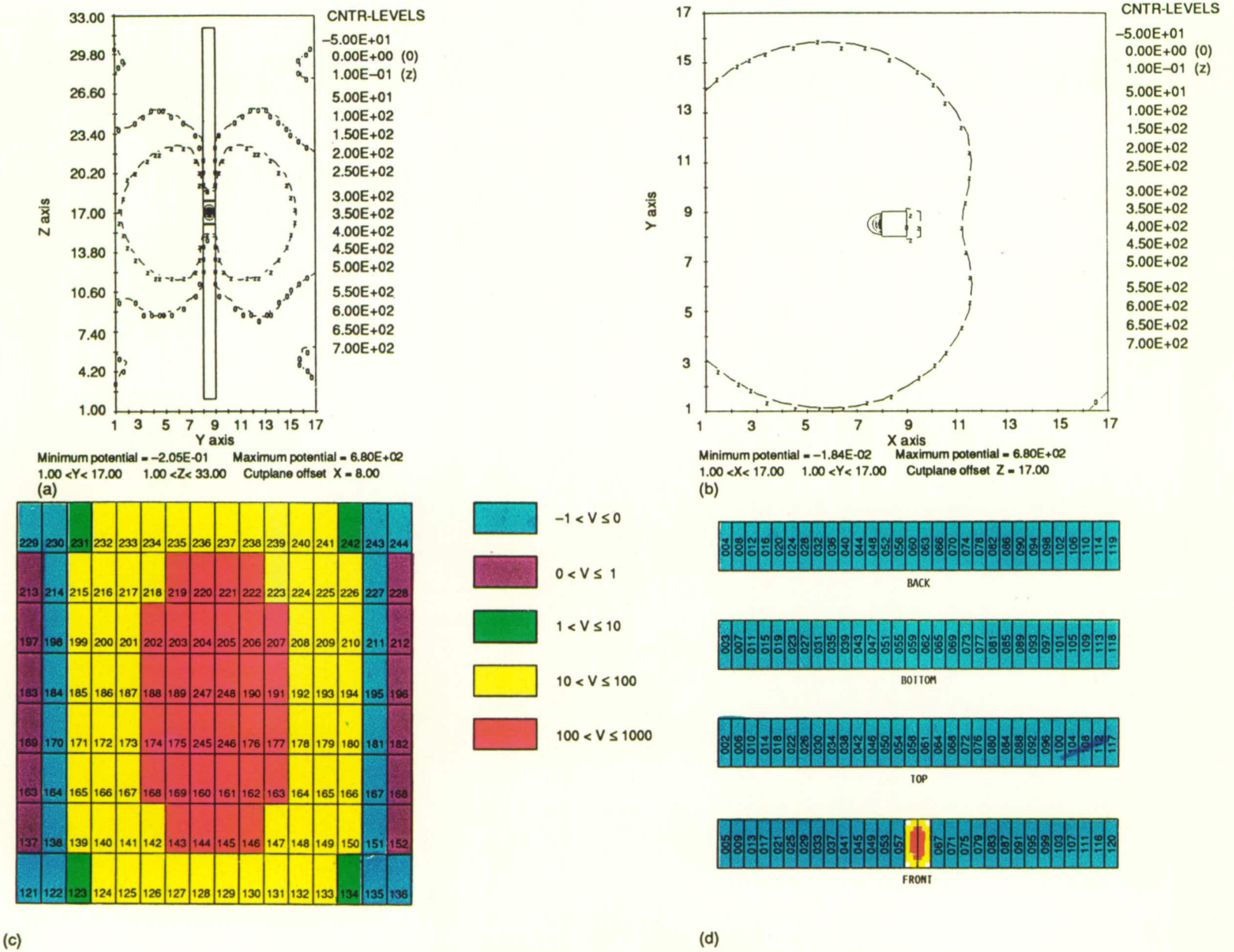

Figure 11.—Contour plots and surface cell potential maps for 680-V NASCAP/LEO run.

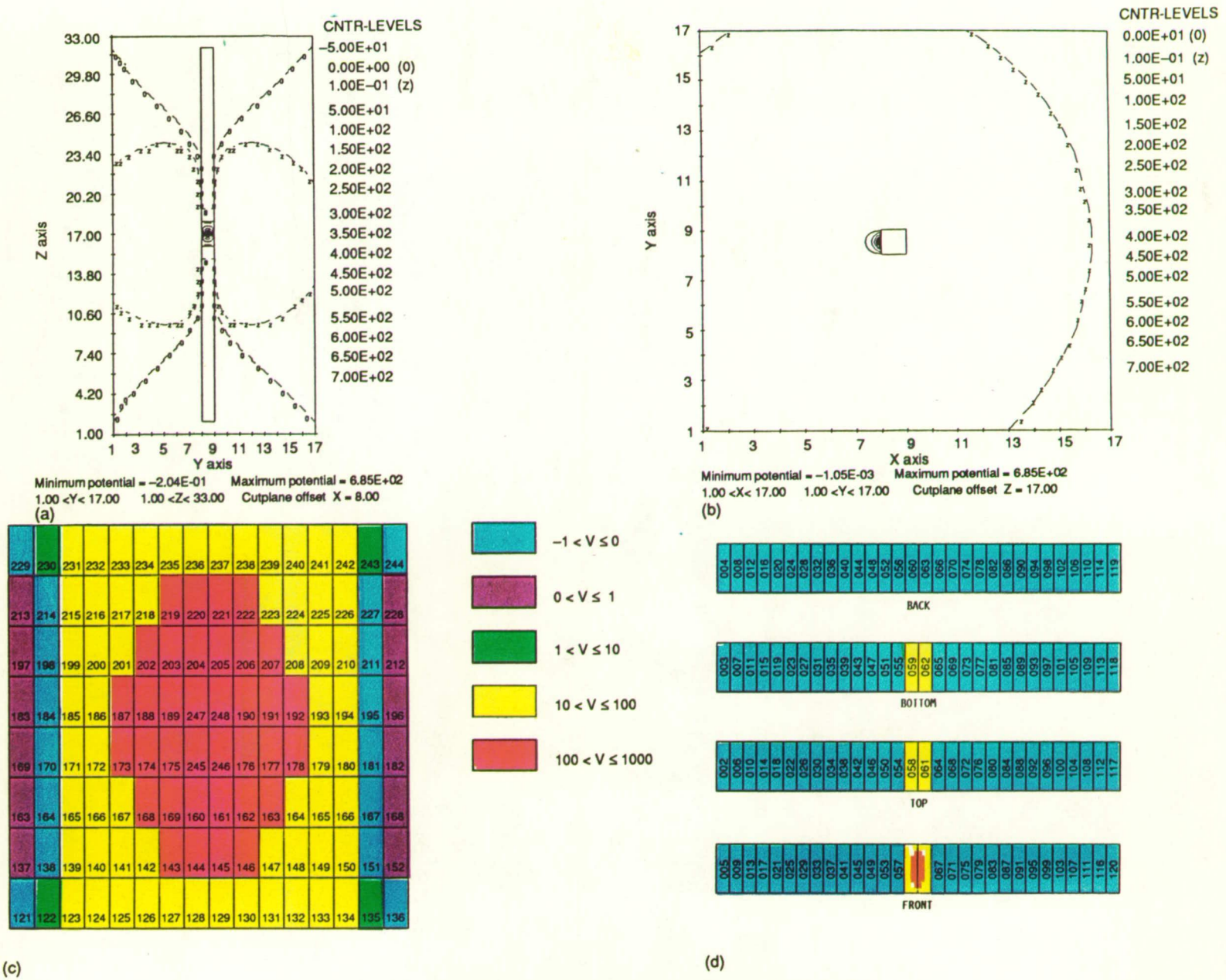

Figure12.—Contour plots and surface cell potential maps for 685-V NASCAP/LEO run.

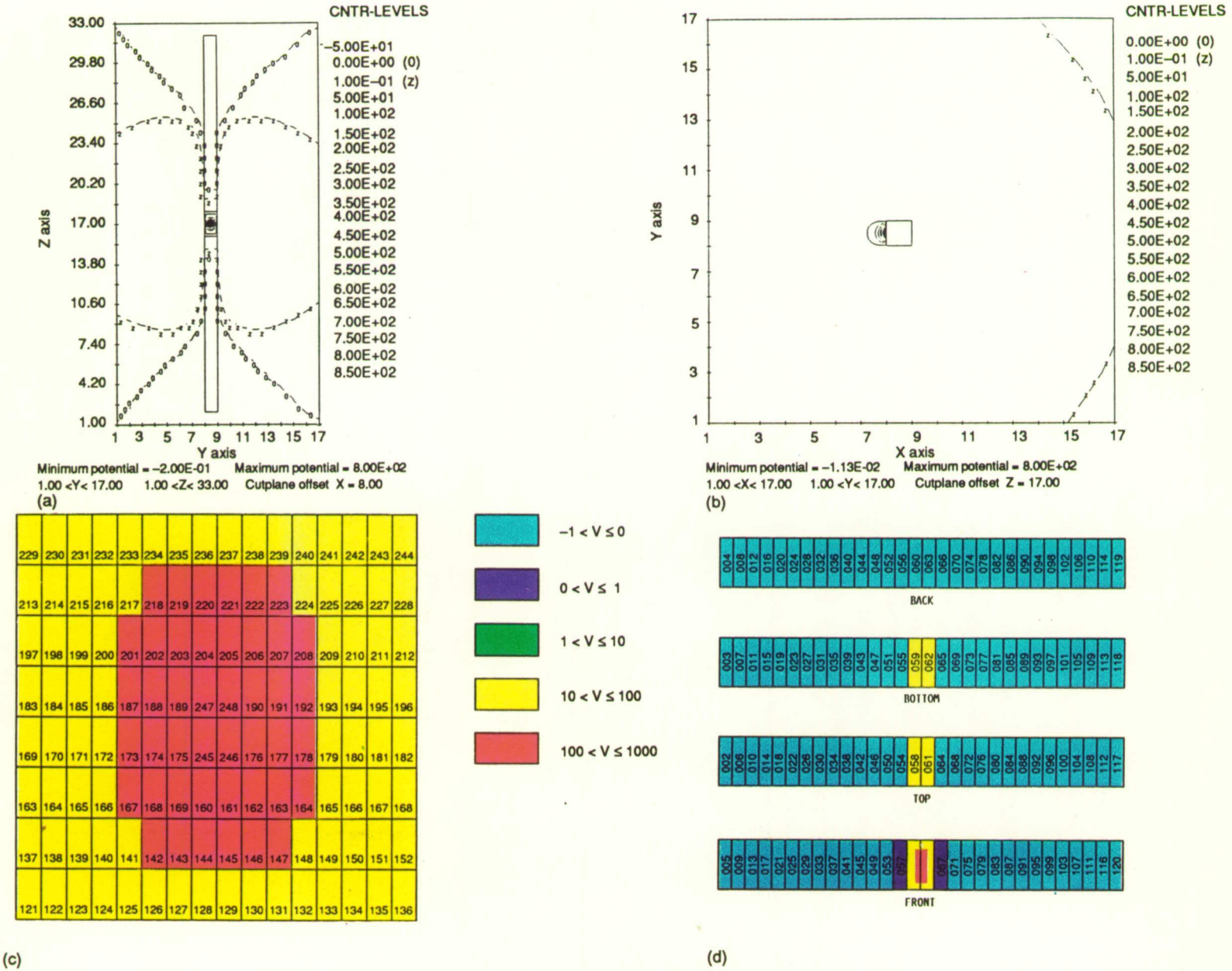

Figure 13.—Contour plots and surface cell potential maps for 800-V NASCAP/LEO run.

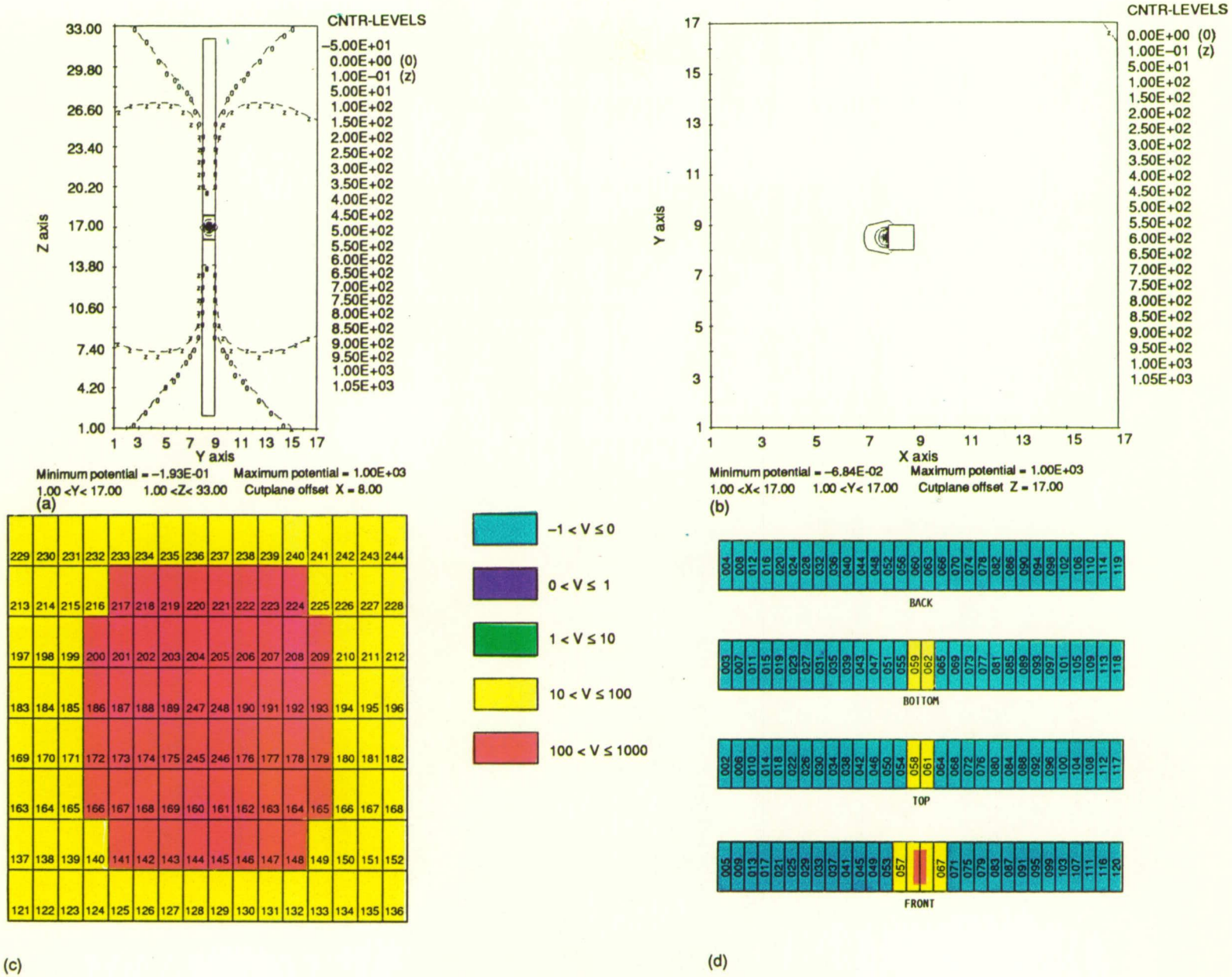

Figure 14.—Contour plots and surface cell potential maps for 1000-V NASCAP/LEO run.

NASA
National Aeronautics and Space Administration

Report Documentation Page

1. Report No.	2. Government Accession No.	3. Recipient's Catalog No.
NASA TM-102486		

4. Title and Subtitle

Comparison of Currents Predicted by NASCAP/LEO Model Simulations With Elementary Langmuir-Type Bare Probe Models for an Insulated Cable Containing a Single Pinhole

5. Report Date

July 1990

6. Performing Organization Code

7. Author(s)

Joel T. Galofaro

8. Performing Organization Report No.

E-5095

10. Work Unit No.

506-41-3K

9. Performing Organization Name and Address

National Aeronautics and Space Administration
Lewis Research Center
Cleveland, Ohio 44135-3191

11. Contract or Grant No.

13. Type of Report and Period Covered

Technical Memorandum

12. Sponsoring Agency Name and Address

National Aeronautics and Space Administration
Washington, D.C. 20546-0001

14. Sponsoring Agency Code

15. Supplementary Notes

16. Abstract

The behavior of a defect in the insulation of a short biased section of cable in a Low Earth Orbit (LEO) space environment was examined. Such studies are of the utmost importance for large space power systems where great quantities of cabling will be deployed. An insulated probe containing a pinhole was placed into a hypothetical high-density LEO plasma. The NASA Charging Analyzer Program (NASCAP/LEO) was used to explore sheath growth about the probe as a function of applied voltage and to predict I-V behavior. A set of independent current calculations using Langmuir's formulations for concentric spheres and coaxial cylinders were also performed. The case of concentric spheres was here extended to include the case of concentric hemispheres. Several simple Langmuir-type models were then constructed to bracket the current collected by the cable. The space-charge sheath radius and impact parameters were used to determine the proper current regime. I-V curves were plotted for the models and comparisons were made with NASCAP/LEO results. Finally, NASCAP/LEO potential contours and surface cell potential plots were examined to explain interesting features in the NASCAP/LEO I-V curve.

17. Key Words (Suggested by Author(s))	18. Distribution Statement
Pinholes in cables; Langmuir-type bare probe theory; High-density LEO plasma; Cable simulation (NASCAP/LEO); NASA charging analyzer program; Charge sheaths; Orbit-limited current collection; Space-charge-limited current collection	Unclassified – Unlimited Subject Category 18

19. Security Classif. (of this report)	20. Security Classif. (of this page)	21. No. of pages	22. Price*
Unclassified	Unclassified	40	A03

NASA FORM 1626 OCT 86

*For sale by the National Technical Information Service, Springfield, Virginia 22161